

## Anharmonic lattice statics analysis of $180^\circ$ and $90^\circ$ ferroelectric domain walls in $\text{PbTiO}_3$

A. YAVARI\*† M. ORTIZ‡  
and K. BHATTACHARYA‡

†School of Civil and Environmental Engineering, Georgia  
Institute of Technology, Atlanta, Georgia 30332

‡Division of Engineering and Applied Science, California  
Institute of Technology, Pasadena, CA 91125

(Received 10 October 2005; in final form 24 April 2007)

This paper presents an anharmonic lattice statics analysis of  $180^\circ$  and  $90^\circ$  domain walls in tetragonal ferroelectric perovskites. We present all the calculations and numerical examples for the technologically important ferroelectric material  $\text{PbTiO}_3$ . We use shell potentials that are fitted to quantum mechanics calculations. Our formulation places no restrictions on the range of the interactions. This formulation of lattice statics is inhomogeneous and accounts for the variation of the force constants near defects. The discrete governing equations for perfect domain walls are reduced using symmetry conditions. We solve the linearized discrete governing equations directly using a novel method in the setting of the theory of difference equations. We calculate the fully nonlinear solutions using modified Newton–Raphson iterations.

### 1. Introduction

Ferroelectrics are polar crystals whose spontaneous polarization vector can be switched by an applied electric field or an external mechanical stress. These materials have many potential applications in micro-actuators and micro-sensors. The phenomenon of ferroelectricity was discovered in 1921 [1] and since then has been the subject of many theoretical and experimental investigations. Ferroelectricity is a result of the fairly complicated competition of short-range repulsive forces that favour the paraelectric state (high symmetry cubic phase) and long-range Coulombic forces that favour the ferroelectric state (low symmetry phase) [2]. Recent applications of ferroelectrics, especially MEMS applications, have attracted much attention in understanding the fundamentals of ferroelectrics. For recent reviews see [3–5].

It is known that many properties of ferroelectrics are controlled by domain walls, which are two-dimensional defects. This is not surprising as many of the interesting properties of solids, in general, are controlled by defects and their evolution. Macroscopically, a domain wall can be understood as a surface of discontinuity in

---

\*Corresponding author. Email: arash.yavari@ce.gatech.edu

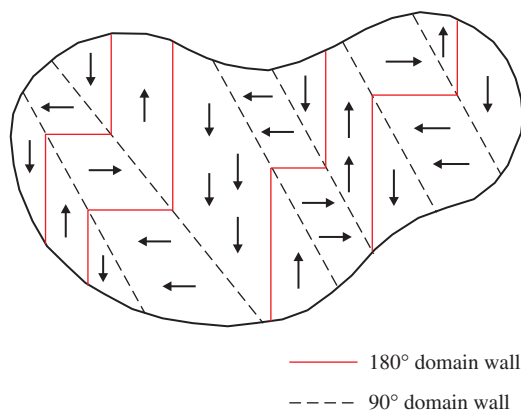


Figure 1. 180° and 90° domain walls.

polarization (polarization per unit volume) and deformation gradient. However, they have an atomistic structure which determines their energy and mobility, and therefore, understanding the atomic structure of ferroelectric domain walls is important. A vast majority of atomistic analyses of domain walls conducted to date are numerical in nature and contain severe restrictions on the size of the computational domain. The present work provides an alternative semi-analytical approach based on lattice statics that overcomes some of the limitations inherent to computational techniques. In particular, the present approach enables consideration of infinite regions, thus furnishing solutions that are free of spurious finite-cell effects.

There are two types of domain walls in the tetragonal  $ABO_3$  perovskites: 90° and 180° domain walls. Examples are shown in figure 1. Note that the 90° domain walls shown in this figure are head-to-tail. This means that the domain wall is free of surface charges. In this paper, we study only head-to-tail 90° domain walls as they have a lower energy compared to other types of 90° domain walls. For more details on different properties of  $BaTiO_3$  and  $PbTiO_3$  the reader may refer to [6, 7].

Stemmer *et al.* [8] measured the width of 90° domain walls in tetragonal  $PbTiO_3$  to be  $1.0 \pm 0.3$  nm and the energy per unit area of the wall to be  $50 \text{ mJ m}^{-2}$ . Floquet *et al.* [9] measured the width of 90° domain walls in tetragonal  $BaTiO_3$  to be 4–6 nm. Foeth *et al.* [10] measured the thickness of 90° domain walls in  $PbTiO_3$  to be  $1.5 \pm 0.3$  nm and  $2.1 \pm 0.7$  nm using HREM and WBTEM, respectively. Recently, Shilo *et al.* [11] studied the structure of 90° domain walls in  $PbTiO_3$  by measuring the surface profile close to emerging domain walls and then fitting it to the soliton-type solution of LGD theory. Using this technique they observed that the domain wall thickness is about 1.5 nm but with a wide scatter. They associated this scatter to point defects. Although there is some scatter in the experimental data available in the literature, there is a consensus on domain walls being atomically sharp.

The structure of ferroelectric domain walls in the continuum scale has been investigated using Landau–Ginzburg–Devonshire theory (LGD) (see [12–14] and references therein). While these calculations are useful to understand the overall structure, they are limited in their ability to capture the structure of atomically sharp ferroelectric domain walls.

Lawless [15] performed an atomistic analysis of  $180^\circ$  domain walls in  $\text{BaTiO}_3$  using a point-dipole model by making a series of simplifying assumptions: the elastic energy (due to changes in lattice parameters) is neglected, only Ti- $\text{O}_a$  ( $\text{O}_a$  in Slater's notation<sup>†</sup>) bonds are considered and only the magnitude of the polarization vector varies across the domain wall. He considered the  $180^\circ$  domain walls perpendicular to the experimentally observed  $\langle 100 \rangle$  and  $\langle 110 \rangle$  directions and analysed four possible domain walls two of which are Ba-centred and the other two are Ti-centred. Finally, he showed that the Ba-centred wall  $(100)$  has the minimum energy.

There have also been several *ab initio* analyses of ferroelectric domain walls in recent years (see [16–19] and references therein). Meyer and Vanderbilt [16] showed that  $180^\circ$  and  $90^\circ$  domain walls in the tetragonal  $\text{PbTiO}_3$  have comparable widths and that the energy barrier for movement of  $90^\circ$  domain walls is extremely small. They discussed different possibilities for  $180^\circ$  and  $90^\circ$  domain walls. There are two types of  $180^\circ$  domain walls: Pb-centred and Ti-centred, which result from twinning on PbO- and  $\text{TiO}_2$ -planes, respectively. They showed that a Pb-centred domain wall has a lower energy than a Ti-centred domain wall and hence it is the preferred wall structure.<sup>‡</sup> For  $90^\circ$  domain walls there are two possibilities: Pb-Ti-O- or O-O-centred domain walls. Here by an O-O-centred domain wall we mean that the reference (starting) configuration is obtained by twinning on an O-O type  $(101)$  plane. Meyer and Vanderbilt observed that the relaxed configuration lies between these two limits. They obtained the profiles of polarization change across the domain wall and calculated the domain wall energies. They also observed that the energy of a  $90^\circ$  domain wall is one-fourth of that of a  $180^\circ$  domain wall. In their computations, Meyer and Vanderbilt had to consider a completely periodic system in order to be able to perform their quantum mechanical calculations. The same superficial periodicity is assumed in all the existing molecular dynamics simulations of ferroelectrics. This is potentially a severe limitation in ferroelectrics because of the presence of long-range electrostatic interactions.

In this paper, we present an anharmonic lattice statics study of  $90^\circ$  and  $180^\circ$  domain walls. Lattice statics has been widely used to study harmonic crystals. The method was introduced by Matsubara [20] and Kanazaki [21]. For more details and history the reader may refer to [22–24] and references therein. Our starting point is an atomistic model of ferroelectric materials based on shell-type atomistic potentials that have been fit to quantum mechanics. Our method is capable of studying infinite domains, and thus does not require any artificial cut off or periodicity. Therefore, we are able to study an isolated domain wall.

In our lattice statics analysis, we start with a reference or trial configuration that contains a domain wall, and look for an equilibrium close to it. The reference configuration is obtained by patching together two half crystals with appropriate relative rotations. We linearize the equilibrium equations about this state and solve these equations semi-analytically by requiring the solutions to be bounded at infinity. The anharmonic or nonlinear solutions are obtained by iteration.

---

<sup>†</sup> $\text{O}_a$  is  $\text{O}_3$  in our notation.

<sup>‡</sup>Our lattice statics calculations are in agreement with this.

This paper is organized as follows. Section 2 discusses shell potentials for modelling polarizability. Section 3 presents a detailed lattice statics analysis of  $180^\circ$  domain walls. Construction of discrete governing equations, their linearization and solution techniques are explained. This is then followed by some numerical examples for  $\text{PbTiO}_3$ . In Section 4 we study the same problems for  $90^\circ$  domain walls. Finally, conclusions are given in Section 5. In the appendix, some issues in systems of charges like long-range forces, etc. are discussed. The method of Wolf *et al.* [25] is critically reviewed for shell potentials and is numerically studied for  $\text{PbTiO}_3$ .

## 2. Total energy of a ferroelectric solid

### 2.1. Shell models

Ferroelectric perovskites have a fairly complicated electronic structure and bonding, which include covalent bonds, but individual atoms may also be ionized and polarized due to distortions in their electron orbitals. Therefore, ferroelectrics are often modelled using shell potentials originally introduced by Dick and Overhauser [26]. In shell models [27–29] it is assumed that an atom is composed of a core, which consists of the nucleus and the inner electrons and a massless shell, which consists of the valence electrons. In shell models, the total energy of the system is assumed to have the following form

$$\mathcal{E} = \mathcal{E}_{\text{short-range}} + \mathcal{E}_{\text{long-range}} + \mathcal{E}_{\text{core-shell}}. \quad (1)$$

The short-range interactions are between the massless shells and in general not all shells contribute to this energy. The long range interactions are Coulomb interactions. The third part of the energy is the energy of interaction of core and shell of the same atom.

It is assumed that the short-range energy is pairwise and is equal to  $\Phi(|\mathbf{x}I^i - \mathbf{x}J^j|)$  for atoms  $I(i)$  and  $J(j)$  for some given scalar-valued function  $\Phi$ . Consider a multilattice  $\mathcal{L}$  with  $N$  species and let  $i \in \mathbb{Z}^3$  denote the unit cell index and  $I \in \{1, \dots, N\}$  denote the sub-lattice number. Consider the  $I(i)$  atom: its core has position  $\mathbf{x}I^i$  and charge  $QI_c^i$  while its shell has position  $\mathbf{x}I_s^i$  and charge  $QI_s^i$ . Thus, the total short-range energy of the system can be written as

$$\mathcal{E}_{\text{short-range}} = \frac{1}{4} \sum_{I, J=1}^N \sum_{i, j} \Phi(|\mathbf{x}I^i - \mathbf{x}J^j|). \quad (2)$$

The core-shell energy is only a function of core and shell positions and has the following form

$$\mathcal{E}_{\text{core-shell}} = \sum_{I=1}^N \sum_i \Upsilon(QI_c^i, QI_s^i), \quad (3)$$

for some function  $\Upsilon$ .

The long-range energy is the Coulombic energy and is a function of both charges and positions of cores and shells and can be written as

$$\begin{aligned} \mathcal{E}_{\text{long-range}} = & \frac{1}{4} \sum_{I,J=1}^N \sum_{i,j} \left\{ \Psi(|\mathbf{x}I^i - \mathbf{x}I_s^j|, QI_c, QI_s^j) \right. \\ & + \Psi(|\mathbf{x}I^i - \mathbf{x}J^j|, QI_c, QJ_c) + \Psi(|\mathbf{x}I^i - \mathbf{x}J_s^j|, QI_c, QJ_s^j) \\ & + \Psi(|\mathbf{x}I_s^i - \mathbf{x}J^j|, QI_s^i, QJ_c) + \Psi(|\mathbf{x}I_s^i - \mathbf{x}J_s^j|, QI_s^i, QJ_s^j) \\ & \left. + \Psi(|\mathbf{x}J^i - \mathbf{x}J_s^j|, QJ_c, QJ_s^j) \right\}, \end{aligned} \quad (4)$$

where a general function  $\Psi$  is assumed in order to include modified shell potentials if necessary. It is assumed that core and shell of an atom do not interact electrostatically. The total energy can be written as

$$\begin{aligned} \mathcal{E} = & \frac{1}{4} \sum_{I,J=1}^N \sum_{i,j} \Phi(|\mathbf{x}I^i - \mathbf{x}J^j|) + \sum_{I=1}^N \sum_i \Upsilon(QI_c, QI_s^i) \\ & + \frac{1}{4} \sum_{I,J=1}^N \sum_{i,j} \left\{ \Psi(|\mathbf{x}I^i - \mathbf{x}J_s^j|, QI_c, QJ_s^j) + \Psi(|\mathbf{x}I^i - \mathbf{x}J^j|, QI_c, QJ_c) \right. \\ & + \Psi(|\mathbf{x}I^i - \mathbf{x}I_s^j|, QI_c, QI_s^j) + \Psi(|\mathbf{x}I_s^i - \mathbf{x}J^j|, QI_s^i, QJ_c) \\ & \left. + \Psi(|\mathbf{x}I_s^i - \mathbf{x}J_s^j|, QI_s^i, QJ_s^j) + \Psi(|\mathbf{x}J^i - \mathbf{x}J_s^j|, QJ_c, QJ_s^j) \right\}. \end{aligned} \quad (5)$$

Note that this energy should be minimized subject to charge conservation constraint, which reads

$$\sum_I \sum_i (QI_c + QI_s^i) = 0. \quad (6)$$

Throughout this work we assume that all charges are fixed.

The potential we use for  $PbTiO_3$  is a classical shell model developed in [27–29]. In the potential of Sepiarsky *et al.* [27] (we call it the SC potential from here on) the short-range interactions are between shells of the pairs Pb-O, Pb-Ti and O-O, with the following forms

$$\text{Pb} - \text{Ti}, \text{Pb} - \text{O}, \text{Ti} - \text{O}: \quad V_{IJ}(r) = (a_{IJ} + b_{IJ}r)e^{-\frac{r}{\rho_{IJ}}}, \quad (7)$$

$$\text{O} - \text{O}: \quad V_{33}(r) = a_{33}e^{-\frac{r}{\rho_{33}}} + \frac{c_{33}}{r^6}, \quad (8)$$

where  $a_{IJ}, b_{IJ}, \rho_{IJ}, c_{33}$  are material properties. The core-shell coupling is anharmonic but isotropic with the following form

$$V_I(\mathbf{x}I_c^i, \mathbf{x}I_s^i) = \frac{1}{2}c_{2I}|\mathbf{x}I^i - \mathbf{x}I_s^i|^2 + \frac{1}{24}c_{4I}|\mathbf{x}I^i - \mathbf{x}I_s^i|^4. \quad (9)$$

**2.1.1. Governing equilibrium equations.** We obtain the governing equilibrium equations for  $\mathbf{x}I^i$  and  $\mathbf{x}I_s^i$  by minimizing the energy (5) with respect to these two variables. The governing equilibrium equations are

$$\delta\mathcal{E}(\{\mathbf{x}I^i, \mathbf{x}I_s^i\}) = 0 \Rightarrow \mathbf{D}_1\mathcal{E} = \mathbf{D}_2\mathcal{E} = \mathbf{0}, \quad (10)$$

or

$$\mathbf{f}(\mathbf{x}I^i, \mathbf{x}I_s^i) = \mathbf{0} \quad \forall i = 1, 2, \dots, I = 1, \dots, N, \quad (11)$$

$$\mathbf{g}(\mathbf{x}I^i, \mathbf{x}I_s^i) = \mathbf{0} \quad \forall i = 1, 2, \dots, I = 1, \dots, N, \quad (12)$$

where

$$\mathbf{f}(\mathbf{x}I^i, \mathbf{x}I_s^i) = \mathbf{D}_1\mathcal{E}(\mathbf{x}I^i, \mathbf{x}I_s^i), \quad (13)$$

$$\mathbf{g}(\mathbf{x}I^i, \mathbf{x}I_s^i) = \mathbf{D}_2\mathcal{E}(\mathbf{x}I^i, \mathbf{x}I_s^i). \quad (14)$$

**2.1.2. Linearized equilibrium equations.** We now linearize the governing equations (11) and (12) about a reference configuration  $\mathcal{B}_0 = (\mathbf{x}I_0^i, \mathbf{x}I_{s0}^i)$  as follows

$$\begin{aligned} &\mathbf{f}(\mathbf{x}I_0^i, \mathbf{x}I_{s0}^i) + \mathbf{D}_1\mathbf{f}(\mathbf{x}I_0^i, \mathbf{x}I_{s0}^i) \cdot (\mathbf{x}I^i - \mathbf{x}I_0^i) \\ &\quad + \mathbf{D}_2\mathbf{f}(\mathbf{x}I_0^i, \mathbf{x}I_{s0}^i) \cdot (\mathbf{x}I_s^i - \mathbf{x}I_{s0}^i) \\ &\quad + o(\|\mathbf{x}I^i - \mathbf{x}I_0^i\|, \|\mathbf{x}I_s^i - \mathbf{x}I_{s0}^i\|) = 0, \end{aligned} \quad (15)$$

$$\begin{aligned} &\mathbf{g}(\mathbf{x}I_0^i, \mathbf{x}I_{s0}^i) + \mathbf{D}_1\mathbf{g}(\mathbf{x}I_0^i, \mathbf{x}I_{s0}^i) \cdot (\mathbf{x}I^i - \mathbf{x}I_0^i) \\ &\quad + \mathbf{D}_2\mathbf{g}(\mathbf{x}I_0^i, \mathbf{x}I_{s0}^i) \cdot (\mathbf{x}I_s^i - \mathbf{x}I_{s0}^i) \\ &\quad + o(\|\mathbf{x}I^i - \mathbf{x}I_0^i\|, \|\mathbf{x}I_s^i - \mathbf{x}I_{s0}^i\|) = 0. \end{aligned} \quad (16)$$

We emphasize that the reference configuration need not be in equilibrium, and therefore we retain the zeroth order term. Thus

$$\mathbf{D}_1\mathbf{f}(\mathbf{x}I_0^i, \mathbf{x}I_{s0}^i) \cdot \mathbf{u}I^i + \mathbf{D}_2\mathbf{f}(\mathbf{x}I_0^i, \mathbf{x}I_{s0}^i) \cdot \mathbf{u}I_s^i = -\mathbf{f}(\mathbf{x}I_0^i, \mathbf{x}I_{s0}^i), \quad (17)$$

$$\mathbf{D}_1\mathbf{g}(\mathbf{x}I_0^i, \mathbf{x}I_{s0}^i) \cdot \mathbf{u}I^i + \mathbf{D}_2\mathbf{g}(\mathbf{x}I_0^i, \mathbf{x}I_{s0}^i) \cdot \mathbf{u}I_s^i = -\mathbf{g}(\mathbf{x}I_0^i, \mathbf{x}I_{s0}^i), \quad (18)$$

where

$$\mathbf{u}I^i = \mathbf{x}I^i - \mathbf{x}I_0^i, \quad \mathbf{u}I_s^i = \mathbf{x}I_s^i - \mathbf{x}I_{s0}^i. \quad (19)$$

For a given reference configuration, the above equations give a system of linear difference equations for the discrete fields of core and shell position vectors.

**2.1.3. Defective crystals and symmetry reduction.** It may happen that a given defective crystal has a partial symmetry. Defective crystals can be classified into three groups [30]: (i) with 1-D symmetry reduction (defective crystals with two-dimensional translation symmetry), (ii) with 2-D symmetry reduction (defective crystals with one-dimensional translation symmetry) and (iii) with no symmetry reduction. Examples of (i), (ii) and (iii) are free surfaces, dislocations, and point

defects, respectively. By convention, a perfect crystal is a defective crystal with 0-D symmetry reduction, i.e. it can be reduced to a unit cell.

Assuming that the defective crystal  $\mathcal{L}$  has a 1-D symmetry reduction, i.e. it can be partitioned into two-dimensional equivalence classes, the neighbouring set  $\mathcal{S}_i$  (the set of atoms that interact with atom  $i$ ) is partitioned as

$$\mathcal{S}_i = \bigsqcup_{\alpha \in \mathbb{Z}} \bigsqcup_{I=1}^N \mathcal{S}_{I\alpha}(i), \tag{20}$$

where  $\mathcal{S}_{I\alpha}(i)$  is the equivalence class of all the atoms of type  $I$  and index  $\alpha$  with respect to atom  $i$ . As an example, for a free surface each equivalence class is a set of atoms lying on a plane parallel to the free surface. Using this partitioning one can write

$$\sum_{j \in \mathcal{S}_i} \frac{\partial^2 \mathcal{E}}{\partial \mathbf{x}^j \partial \mathbf{x}^i}(\mathcal{B}_0)(\mathbf{x}^j - \mathbf{x}^i) = \sum'_{\alpha=-\infty}^{\infty} \sum_{I=1}^N \sum_{j \in \mathcal{S}_{I\alpha}(i)} \frac{\partial^2 \mathcal{E}}{\partial \mathbf{x}^j \partial \mathbf{x}^i}(\mathcal{B}_0)(\mathbf{x}^{I\alpha} - \mathbf{x}_0^{I\alpha}), \tag{21}$$

where the prime in the first sum in the right-hand side means that the term  $\alpha = 0, I = i$  is omitted. We are interested in planar defects that have two dimensions of translational symmetry. Therefore, we partition the lattice into planes perpendicular to the defect (indexed by  $\alpha$ ), and carry out all sums first with  $\alpha$  fixed and then over all  $\alpha$ . The linearized discrete governing equations can be written as

$$\sum'_{\alpha=-\infty}^{\infty} \sum_{I=1}^N \mathbf{K}_{iI\alpha} \mathbf{u}^{I\alpha} + \left( - \sum'_{\alpha=-\infty}^{\infty} \sum_{I=1}^N \mathbf{K}_{iI\alpha} \right) \mathbf{u}^i = \mathbf{f}_i, \tag{22}$$

where

$$\mathbf{K}_{iI\alpha} = \sum_{j \in \mathcal{S}_{I\alpha}(i)} \frac{\partial^2 \mathcal{E}}{\partial \mathbf{x}^j \partial \mathbf{x}^i}(\mathcal{B}_0), \tag{23}$$

$$\mathbf{f}_i = - \frac{\partial \mathcal{E}}{\partial \mathbf{x}^i}(\mathcal{B}_0) + \mathbf{F}_i, \tag{24}$$

$$\mathbf{u}^{I\alpha} = \mathbf{x}^{I\alpha} - \mathbf{x}_0^{I\alpha} = \mathbf{x}^j - \mathbf{x}_0^j \quad \forall j \in \mathcal{S}_{I\alpha}(i), \tag{25}$$

and  $\mathbf{F}_i$  is the external applied force on atom  $\mathbf{x}^i$ . Unit cell displacement vectors are defined as

$$\mathbf{X}_n = \begin{pmatrix} \mathbf{u}_n^1 \\ \vdots \\ \mathbf{u}_n^N \end{pmatrix}. \tag{26}$$

Now the governing equations in terms of unit cell displacements are

$$\sum_{\alpha=-\infty}^{\infty} \mathbf{A}_{\alpha}(n) \mathbf{X}_{n+\alpha} = \mathbf{F}_n \quad n \in \mathbb{Z}, \quad (27)$$

where

$$\mathbf{A}_{\alpha}(n) \in \mathbb{R}^{3N \times 3N}, \mathbf{X}_{\alpha}, \mathbf{F}_n \in \mathbb{R}^{3N}. \quad (28)$$

This is a linear vector-valued ordinary difference equation with variable coefficient matrices. The unit cell force vectors and the unit cell stiffness matrices are defined as

$$\mathbf{F}_n = \begin{pmatrix} \mathbf{F}_{1n} \\ \vdots \\ \mathbf{F}_{Nn} \end{pmatrix}, \quad \mathbf{A}_{\alpha}(n) = \begin{pmatrix} \mathbf{K}_{11\alpha} & \mathbf{K}_{12\alpha} & \cdots & \mathbf{K}_{1N\alpha} \\ \mathbf{K}_{21\alpha} & \mathbf{K}_{22\alpha} & \cdots & \mathbf{K}_{2N\alpha} \\ \vdots & \vdots & \cdots & \vdots \\ \mathbf{K}_{N1\alpha} & \mathbf{K}_{N2\alpha} & \cdots & \mathbf{K}_{NN\alpha} \end{pmatrix} n \in \mathbb{Z}. \quad (29)$$

Note that the equations (27) are of order infinity. One can make an approximation and assume that each unit cell interacts only with its first  $m$  nearest-neighbour unit cells. The resulting (approximate) difference equation is of the order  $2m + 1$ . The sequence of solutions to these difference equations approaches to the solution of (27) as  $m \rightarrow \infty$  if a solution exists. Sensitivity of solutions to the choice of  $m$  should be numerically studied given an interatomic potential.

## 2.2. Multilattices of $ABO_3$ perovskites

In an  $ABO_3$  crystal, there are three species and five simple sublattices. Throughout this analysis we adopt the following identification

$$A = 1, B = 2, O1 = 3, O2 = 4, O3 = 5, \quad (30)$$

where O1, O2 and O3 are the three simple lattices of oxygen.  $PbTiO_3$  is studied in its tetragonal phase with lattice parameters  $a = b = 3.9053 \text{ \AA}$  and  $c = 4.1514 \text{ \AA}$ . The multilattice of  $ABO_3$  can be defined as

$$\mathcal{L} = \{ \mathbf{x} = v^1 \mathbf{e}_1 + v^2 \mathbf{e}_2 + v^3 \mathbf{e}_3 + \mathbf{p}_i, \quad v^1, v^2, v^3 \in \mathbb{Z}, \quad i = 1, \dots, 5 \}, \quad (31)$$

where  $\mathbf{e}_i, \mathbf{p}_i$  are lattice and shift vectors, respectively. In this paper, we will use a shell model, in which every atom has a core and a shell of electrons that can move independently. This means that for defining the multilattice of cores and shells one needs ten shift vectors. We thus use the following identification

$$\{A_c, A_s, \dots, O3_c, O3_s\} = \{1, 2, \dots, 9, 10\}. \quad (32)$$

**Problem definition.** We seek to find the relaxed configurations of single  $180^\circ$  and  $90^\circ$  domain walls in infinite lattices of  $PbTiO_3$ . Figure 2 shows the two configurations schematically in terms of macroscopic polarization. It is assumed that the far-field conditions are the bulk configurations. In particular, we do not assume any periodicity.



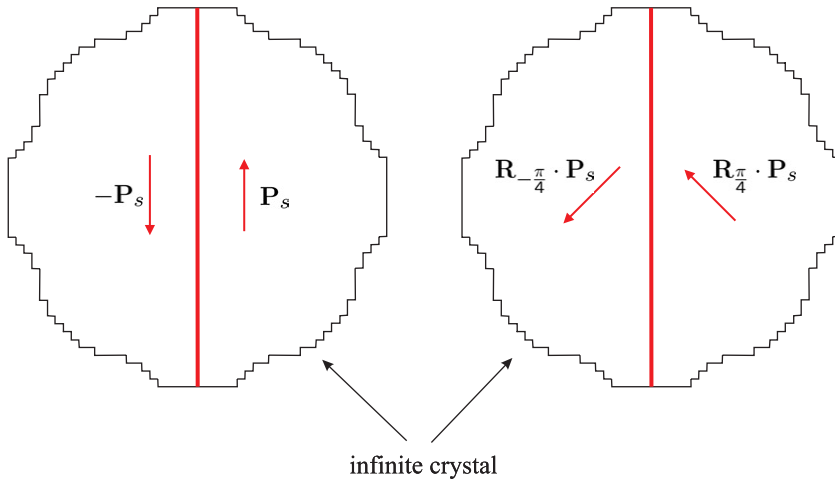


Figure 2. Single  $180^\circ$  and  $90^\circ$  domain walls in infinite crystals with the bulk far-field conditions.  $P_s$  is the spontaneous polarization vector and  $R_{-\pi/4}$  and  $R_{\pi/4}$  are rotation matrices.

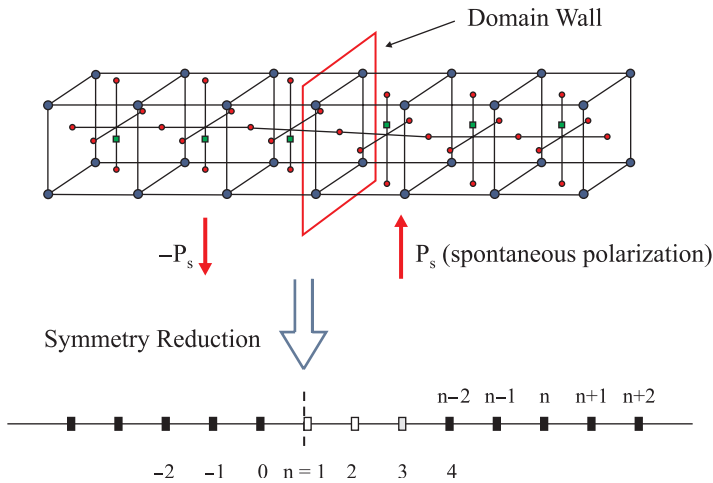


Figure 3. Reference configuration used in analysis of a  $180^\circ$  domain wall.

### 3. $180^\circ$ domain walls in $\text{PbTiO}_3$

We now study the structure of  $180^\circ$  domain walls. Recall that these are planar defects across which the polarization changes by  $180^\circ$ .

The reference configuration is schematically shown in figure 3 for a  $180^\circ$  domain wall. In this problem because of symmetry translation along the wall, it is sufficient to obtain the atomic displacements only in two planes perpendicular to the domain wall. A detailed structure of the reference configuration in these planes denoted by planes (a) and (b) is shown in figure 4. We look for solutions that are periodic in

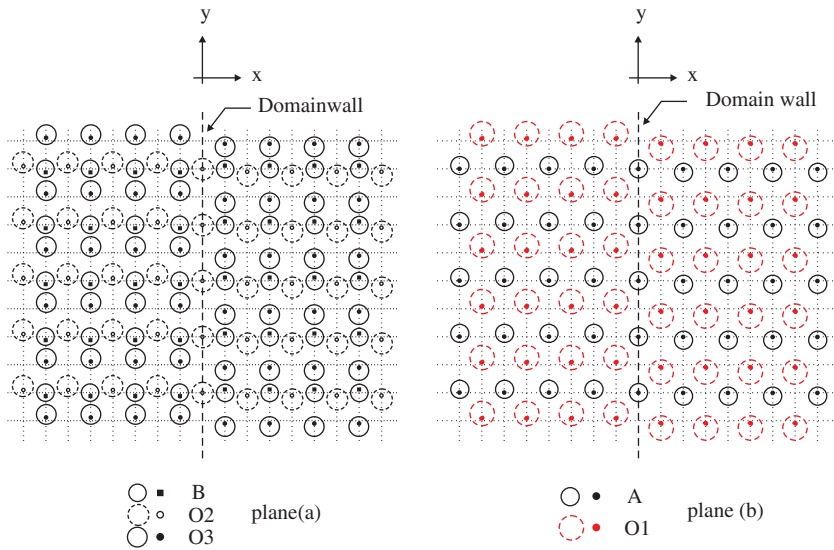
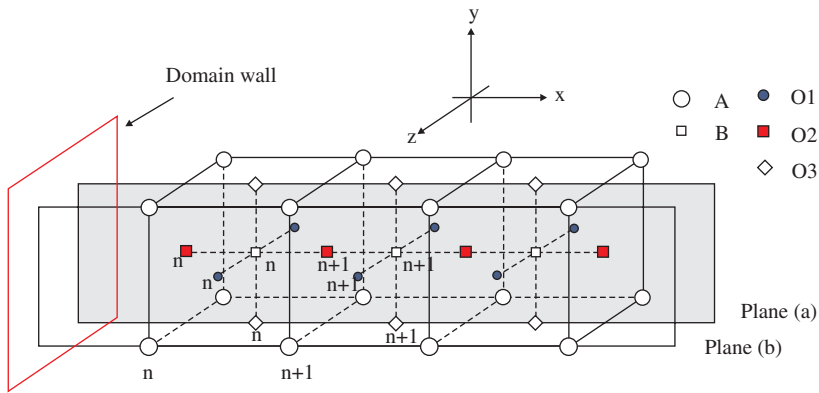


Figure 4. Reference configuration for an A-centred  $180^\circ$  domain wall shown in the two planes (a) and (b). Note that the reference configuration is invariant under the transformation  $x \rightarrow -x, y \rightarrow -y, z \rightarrow z(or -z)$ .

directions along the domain wall. Therefore, we assume that all the atoms of the same type that lie on a plane parallel to the domain wall have the same displacements. Finally, due to the reflection symmetry of a  $180^\circ$  domain wall, we can look at only  $\mathcal{L}^r$ , the half lattice of  $ABO_3$ , i.e. the half space of atoms that lie on the right side of the domain wall including the atoms that lie on the wall.  $\mathcal{L}^r$  can be partitioned into ten pairwise disjoint sublattices, i.e.

$$\mathcal{L}^r = \bigcup_{l=1}^{10} \mathcal{L}_l. \tag{33}$$

Next, each  $\mathcal{L}_I$  is partitioned into subsets according to their distance from the domain wall, i.e.

$$\mathcal{L}_I = \bigcup_{n=0}^{\infty} \mathcal{L}_I(n), \quad (34)$$

where

$$\mathcal{L}_I(n) = \{\mathbf{x} \in \mathcal{L}_I | (\mathbf{x} - \mathbf{p}_I) \cdot \hat{\mathbf{e}}_x = na, \quad n \in \mathbb{N} \cup \{0\}\}, \quad (35)$$

and where  $(\mathbf{x} - \mathbf{p}_I) \cdot \hat{\mathbf{e}}_x$  is the component of  $\mathbf{x} - \mathbf{p}_I$  perpendicular to the domain wall and  $a$  is the lattice spacing.

The electrostatic energy between two charges  $i$  and  $j$  with relative distance  $r$  is  $O(1/r)$  and hence force is  $O(1/r^2)$  and stiffness is  $O(1/r^3)$ . Thus, unbalance forces are represented by lattice sums in  $\mathbb{Z}^3$  with each term being  $O(1/r^2)$ , i.e. each force vector is represented by a conditionally convergent lattice sum and hence one must specify a ‘physically correct’ way of summing the lattice sum. This has been a problem of interest in physics for a very long time. There are methods for calculating the ‘physically correct’ energy or force for such conditionally convergent lattice sums, the most celebrated one being the classical Ewald method [31]. However, for a nonperiodic problem Ewald-type techniques cannot be used. We use a direct-space summation method introduced by Wolf and his co-workers [25]. There are some subtleties in using this method and there are also some mathematical inconsistencies in its original derivation that are discussed in detail in the Appendix.

Each substiffness matrix is defined by a lattice sum (see equation 23). In a domain wall problem, one partitions the defective lattice into equivalent classes of atoms lying on planes parallel to the domain wall. All the atoms (cores or shells) in a given equivalence class displace together and hence it would be enough to calculate the displacement vector of a representative from each class. Therefore, in calculating substiffness matrices representative of a given class interacts with other equivalence classes. This means that given a class, any substiffness matrix is a lattice sum in  $\mathbb{Z}^2$ . Because each term in the lattice sum is  $O(1/r^3)$  and is summed in  $\mathbb{Z}^2$ , the substiffness lattice sums are all absolutely convergent, i.e. the numerically calculated stiffness matrix is insensitive to the way the lattice sum is calculated. For our numerical calculations we use a  $30 \times 30$  square of charges in any equivalence class. Harmonic solutions are insensitive to any larger choice of in-plane stiffness cut-off.

In the previous section, we showed how the linearized governing equations can be written in terms of unit cell forces and displacements. There, we explained that the linearized equations are of infinite order, in general. A ‘formal’ cut-off of unit cell interactions (out-of-plane stiffness cut-off) resulted in a difference equation of order  $2m + 1$  assuming that each unit cell interacts with its first  $m$  nearest neighbour unit cells. One should note that, in general, one is not allowed to ignore higher-order differences (or derivatives in a differential equation). In the domain wall problem, unbalanced forces are always calculated exactly. Using an out-of-plane stiffness cut-off  $m$ , one can solve the resulting finite-order difference equation. This would give a sequence of solutions depending on  $m$ , say  $\{X_m\}_{m=1}^{\infty}$ . Our numerical tests show that for  $m = 1$  and  $m = 2$  solutions are almost the same (they differ by less than 0.5%

and the anharmonic solutions are exactly the same). Thus, we choose  $m = 1$  in all the calculations as this results in stiffness matrices with the least possible ill-conditioning.

We can now obtain the governing equilibrium equations as described earlier. In light of all the symmetry assumptions, we obtain a set of ordinary difference equations. Proceeding to linearize them as also described earlier, we obtain vector-valued ordinary difference equations with the following form

$$\sum_{\alpha=-m}^m \mathcal{A}_\alpha \mathbf{X}_{n+\alpha} = \mathbf{F}_n \quad n \geq m + 1, \quad (36)$$

$$\sum_{\alpha=-m}^m \mathcal{A}_\alpha(n) \mathbf{X}_{n+\alpha} = \mathbf{F}_n \quad n = 0, 1, \dots, m, \quad (37)$$

where  $\mathbf{X}_n \in \mathbb{R}^{30}$  is the displacement vector of unit cell  $n$  and  $\mathbf{F}_n \in \mathbb{R}^{30}$  is the unbalance force vector for the same unit cell.

The matrices  $\mathcal{A}_\alpha$  depend on the reference configuration and, in general, are not symmetric [30, 32]. Boundary equations are the governing equations for the boundary atoms. In this problem, a bulk atom is an atom that does not interact with any atom on the wall or on the left side of the wall. All the other atoms are boundary atoms. For interactions of order  $m$ , boundary atoms are atoms with indices  $n \in \{1, 2, \dots, m\}$ .

We solve (36)–(37) under the assumption that  $\|\mathbf{X}_n\| < \infty$  as  $n \rightarrow \infty$ , i.e. the crystal goes to the bulk structure away from the domain wall. See [30] for a detailed discussion.

Treating the boundary unit cells separately is one of the main features of our inhomogeneous lattice statics. It should also be noted that displacements of the atoms on the left side of the wall are related to those of their corresponding atoms on the right side of the domain wall as will be explained shortly. The discrete boundary-value problem of a  $180^\circ$  domain wall is solved using a direct method presented in [30]. We will see in our numerical calculations that the  $a$ -displacements are an order of magnitude smaller than the corresponding  $c$ -displacements. Here  $a$ -displacements are displacement components perpendicular to the domain wall and  $c$ -displacements are displacements along the tetragonal  $c$ -direction, i.e. parallel to the macroscopic polarization.

Note that because of symmetry, displacements are nonzero only in the tetragonal  $c$ -direction and perpendicular to the domain wall, i.e.  $z$ -components of all displacements are zero. Meyer and Vanderbilt [16] ignore the displacements perpendicular to the domain wall. Here, we make no such assumption and fully relax the defective system.

### 3.1. Anharmonic lattice statics analysis of $180^\circ$ domain walls

Anharmonic lattice statics is based on the Newton–Raphson (NR) method for solving nonlinear equations. The basic idea of NR method is to look at a quadratic approximation to the nonlinear equations in each step. In modified Newton–Raphson method, the Hessian matrix is not updated in each iteration and instead the initial Hessian is used. Modified Newton–Raphson is slowly and linearly

convergent and a large number of iterations should be performed to get good results. In our lattice statics calculations this is an efficient method as the most expensive part of the calculations is the computation of substiffness matrices (very slowly converging lattice sums). The discrete governing boundary-value problem for a  $180^\circ$  domain wall has the following form:

$$\begin{cases} \sum_{\alpha=-m}^m \mathcal{A}_\alpha \mathbf{X}_{n+\alpha} = \mathbf{F}_n, & n \geq m + 2 (m \in \mathbb{N}) \\ \sum_{\alpha=-m}^m \mathcal{A}_\alpha(n) \mathbf{X}_{n+\alpha} = \mathbf{F}_n, & n = 1, \dots, m + 1 \\ \|\mathbf{X}_n\| < \infty & \text{as } n \rightarrow \infty, \end{cases} \quad (38)$$

with the following symmetry relations

$$\mathbf{X}_k = \mathbf{R} \mathbf{X}_{-k+1} + \mathbf{R}' \mathbf{X}_{-k+2} \quad k = -m + 1, \dots, 0, \quad (39)$$

where the matrices  $\mathbf{R}$  and  $\mathbf{R}'$  have the following forms,

$$\mathbf{R} = \begin{pmatrix} \tilde{\mathbf{R}} & \\ & \tilde{\mathbf{R}} \end{pmatrix}, \quad \mathbf{R}' = \begin{pmatrix} \tilde{\mathbf{R}}' & \\ & \tilde{\mathbf{R}}' \end{pmatrix}, \quad (40)$$

where

$$\tilde{\mathbf{R}} = \text{diag}\{\mathbf{0}, -\mathbf{I}, -\mathbf{I}, \mathbf{0}, -\mathbf{I}\}, \quad \tilde{\mathbf{R}}' = \text{diag}\{-\mathbf{I}, \mathbf{0}, \mathbf{0}, -\mathbf{I}, \mathbf{0}\}, \quad \mathbf{I} = \text{diag}\{1, 1, 1\}. \quad (41)$$

In the governing equations  $\mathcal{A}_\alpha(n)$  are the boundary stiffness matrices and explicitly depend on  $n$ . For the first iteration the discrete boundary-value problem determining  $\mathbf{X}^1 = \{\mathbf{X}_n^1\}$  is

$$\begin{cases} \sum_{\alpha=-m}^m \mathcal{A}_\alpha \mathbf{X}_{n+\alpha}^1 = \mathbf{F}_n^0, & n \geq m + 2 (m \in \mathbb{N}) \\ \sum_{\alpha=-m}^m \mathcal{A}_\alpha(n) \mathbf{X}_{n+\alpha}^1 = \mathbf{F}_n^0, & n = 1, \dots, m + 1 \\ \|\mathbf{X}_n^1\| < \infty & \text{as } n \rightarrow \infty. \end{cases} \quad (42)$$

where

$$\mathbf{F}_n^0 = \mathbf{F}_n(\mathcal{B}_0), \quad (43)$$

and  $\mathcal{B}_0$  is the starting configuration (reference configuration).

For the next step

$$\mathcal{B}_1 = \mathcal{B}_0 + \{\mathbf{X}_n^1\}, \quad \mathbf{F}_n^1 = \mathbf{F}_n(\mathcal{B}_1). \quad (44)$$

Now the discrete boundary-value problem determining  $\mathbf{X}^2 = \{\mathbf{X}_n^2\}$  is

$$\begin{cases} \sum_{\alpha=-m}^m \mathcal{A}_\alpha \mathbf{X}_{n+\alpha}^2 = \mathbf{F}_n^1, & n \geq m + 2 (m \in \mathbb{N}) \\ \sum_{\alpha=-m}^m \mathcal{A}_\alpha(n) \mathbf{X}_{n+\alpha}^2 = \mathbf{F}_n^1, & n = 1, \dots, m + 1 \\ \|\mathbf{X}_n^2\| < \infty & \text{as } n \rightarrow \infty. \end{cases} \quad (45)$$

Similarly, the discrete boundary-value problem determining  $\mathbf{X}^{k+1} = \{\mathbf{X}_n^{k+1}\}$  is

$$\begin{cases} \sum_{\alpha=-m}^m \mathcal{A}_\alpha \mathbf{X}_{n+\alpha}^{k+1} = \mathbf{F}_n^k, & n \geq m + 2 (m \in \mathbb{N}) \\ \sum_{\alpha=-m}^m \mathcal{A}_\alpha(n) \mathbf{X}_{n+\alpha}^{k+1} = \mathbf{F}_n^k, & n = 1, \dots, m + 1 \\ \|\mathbf{X}_n^{k+1}\| < \infty & \text{as } n \rightarrow \infty, \end{cases} \quad (46)$$

where

$$\mathcal{B}_k = \mathcal{B}_{k-1} + \{\mathbf{X}_n^k\}, \quad \mathbf{F}_n^k = \mathbf{F}_n(\mathcal{B}_k). \quad (47)$$

It is to be noted that the matrices  $\mathcal{A}_\alpha$  and  $\mathcal{A}_\alpha(n)$  are calculated with reference to  $\mathcal{B}_0$  and remain fixed during all the iterations.

As we do not have control on the reference configuration, in some cases, it may be reasonable to update the stiffness matrices to ensure positive-definiteness of the discrete convolution operator. Because we expect to see localized distortions, the matrices  $\mathcal{A}_\alpha$  will not change and it would be enough to update the boundary stiffness matrices. Now the  $k$ th iteration would have the following form

$$\begin{cases} \sum_{\alpha=-m}^m \mathcal{A}_\alpha \mathbf{X}_{n+\alpha}^{k+1} = \mathbf{F}_n^k, & n \geq m + 2 (m \in \mathbb{N}) \\ \sum_{\alpha=-m}^m \mathcal{A}_\alpha^k(n) \mathbf{X}_{n+\alpha}^{k+1} = \mathbf{F}_n^k, & n = 1, \dots, m + 1 \\ \|\mathbf{X}_n^{k+1}\| < \infty & \text{as } n \rightarrow \infty, \end{cases} \quad (48)$$

where

$$\mathcal{A}_\alpha^k(n) = \mathcal{A}_\alpha(n)(\mathcal{B}_k). \quad (49)$$

We will numerically compare the harmonic and anharmonic solutions in the next subsection.

### 3.2. Numerical results

In this subsection, we report some numerical results for  $\text{PbTiO}_3$ . We compared Pb core harmonic displacements in both Pb-centred and Ti-centred  $180^\circ$  domain walls for different ranges of interaction  $m$  of representative unit cells. We observed that the shell potential is extremely localized. Harmonic solutions for  $m=1$  and  $m=2$  differ by less than 0.5% and the corresponding anharmonic solutions are exactly the same. Therefore, in all the numerical calculations to follow, we use  $m=1$ .

Anharmonic displacements of Pb and O2 in a Pb-centred  $180^\circ$  domain wall are shown in figure 5. Figure 6 shows the corresponding displacements for Ti, O1 and O3 cores and shells.

The anharmonic lattice statics iterations converged after 15 iterations assuming that force tolerance is  $0.05 \text{ eV}/\text{\AA}$ . It is seen that the domain wall thickness is about 1.0 nm in agreement with the *ab initio* calculations [16]. It is seen that core-shell relative displacement of O3 is largest and thus O3 has the most contribution to polarization. Beyond two lattice spacings away from the domain wall all the cores and shells move rigidly and with the same amount, i.e. away from the domain wall the displacement field is a rigid translation. To check the effect of cut-off of difference equations, we compared the anharmonic lattice statics solutions for  $m=1$  and  $m=2$  and observed that their nonlinear solutions are exactly the same. Anharmonic displacements of Pb and O2 cores and shells for a Ti-centred  $180^\circ$  domain wall

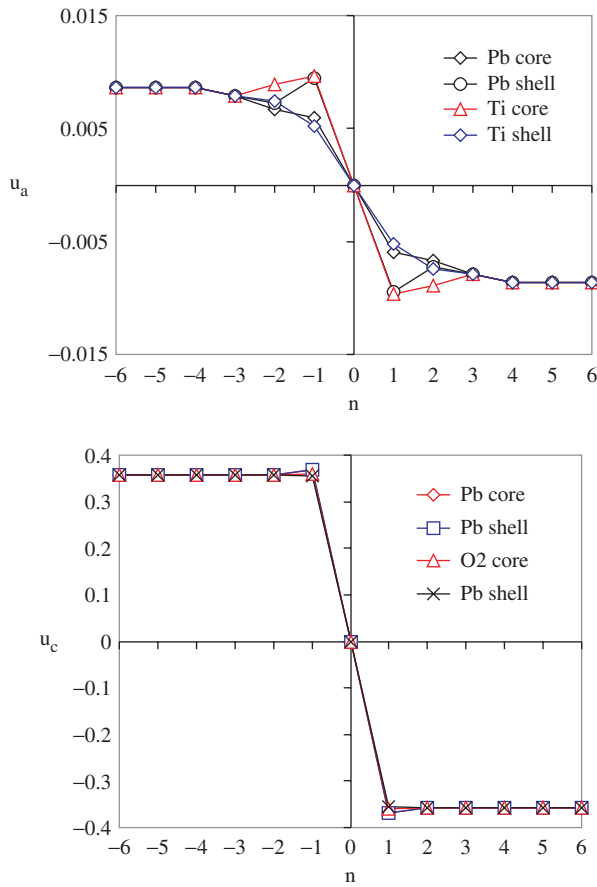


Figure 5. Anharmonic displacements of Pb and O2 cores and shells for a Pb-centred  $180^\circ$  domain wall ( $m=1$ ).

are shown in figure 7. The corresponding displacements for Ti, O1 and O3 are shown in figure 8. Again, it is seen that the domain wall thickness is about 1.0 nm.

In this figure, both  $a$ -displacements and  $c$ -displacements are shown. It is seen that  $a$ -displacements are an order of magnitude smaller than  $c$ -displacements and hence are negligible.

Harmonic and anharmonic polarization profiles for Pb-centred and Ti-centred  $180^\circ$  domain walls are shown in figure 9. The polarization is not defined unambiguously in this scale and we have associated a polarization to each unit cell [33]. For a Pb-centred domain wall, the Pb and O2 displacements are averaged for each unit cell. For a Ti-centred domain wall, the Ti, O1 and O3 displacements are averaged for each unit cell.

Energy calculations show that energies are three orders of magnitude larger than the ones *ab initio* calculations predict. A Ti-centred  $180^\circ$  domain wall has an energy about 40% higher than that of a Pb-centred domain wall. Note that *ab initio* calculations predict that the energy of a Ti-centred domain wall is 30% higher than that of a Pb-centred domain wall.

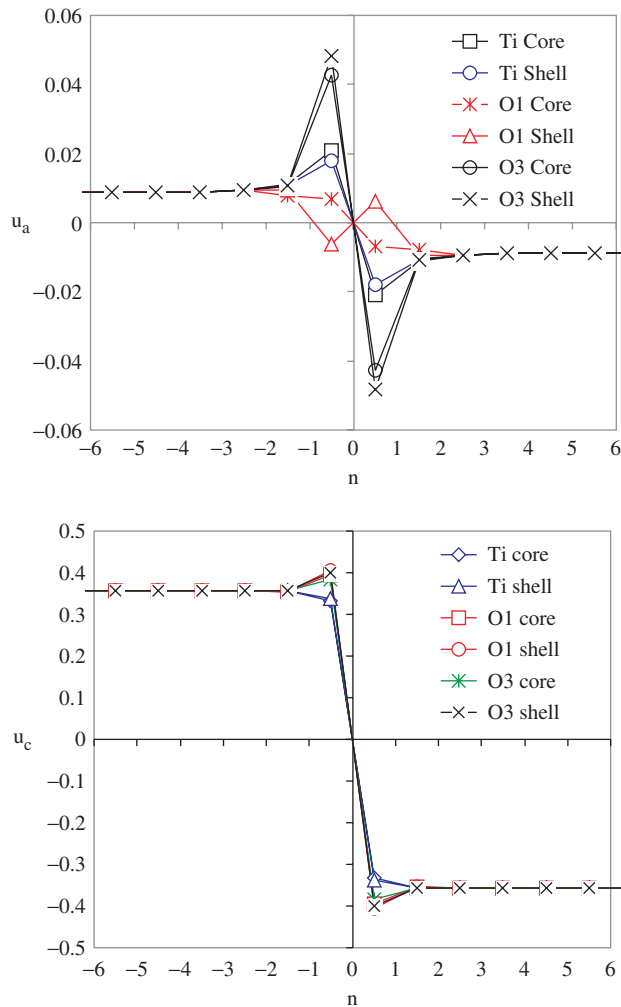


Figure 6. Anharmonic displacements of Ti, O1 and O3 cores and shells for a Pb-centred  $180^\circ$  domain wall ( $m = 1$ ).

#### 4. $90^\circ$ domain walls in $\text{PbTiO}_3$

For the  $90^\circ$  domain wall problem, again it is enough to have the displacements only in two planes. Two obvious possibilities for a  $90^\circ$  domain wall are ABO1-centred and O2O3-centred domain walls. However, one can see that in both these reference configurations all atoms have nonzero unbalanced forces and these can be considered only as two convenient reference configurations, i.e. nominal domain walls.

We start with the ABO1-centred  $90^\circ$  domain wall, although this is just a matter of choice. The reference configuration for A cores and shells is shown in figure 10. Note that this is a nominal domain wall and we are interested in finding the relaxed configuration starting from this reference configuration. Also, note that the problem we are trying to solve is a single  $90^\circ$  domain wall in an infinite lattice. Our numerical



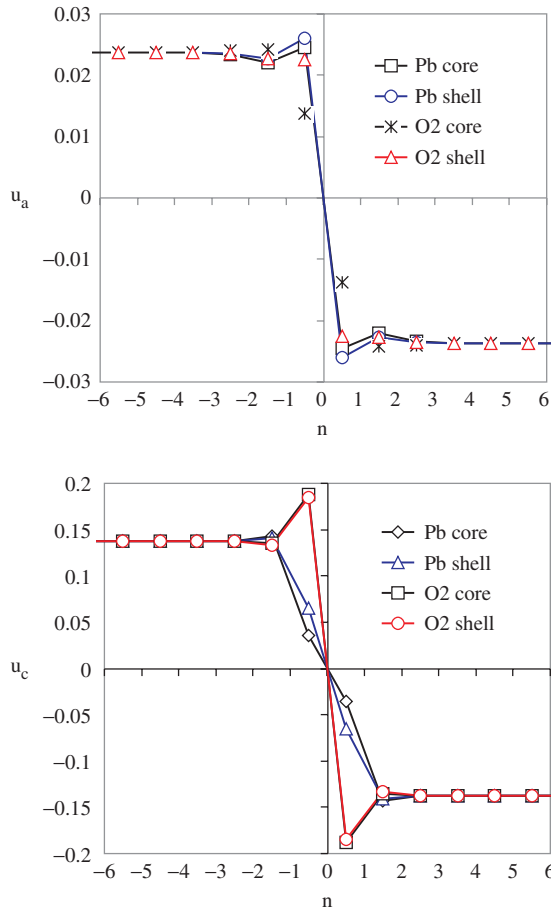


Figure 7. Anharmonic displacements of Pb and O2 cores and shells for a Ti-centred  $180^\circ$  domain wall.

calculations show that the  $a$ -components (perpendicular to the wall) of forces are of the same order as  $c$ -components. However, they decay to zero faster than  $c$ -component of forces.

Reference configuration in two planes (a) and (b) (similar to what is shown in figure 4 for  $180^\circ$  domain walls) is shown in figure 11. It is possible to reduce the governing equations to a 1-D problem, i.e. for each atom type it is enough to have the displacements of cores and shells only on a line perpendicular to the domain wall. In this case the distance between planes of equivalent atoms is

$$\ell = c \sin \theta, \quad \theta = \tan^{-1} \left( \frac{a}{c} \right). \quad (50)$$

Unlike the  $180^\circ$  domain wall problem, there is no symmetry relation between forces and displacements on two sides of the wall. This can be seen in figure 10. This asymmetry implies that we have to solve the governing difference equations

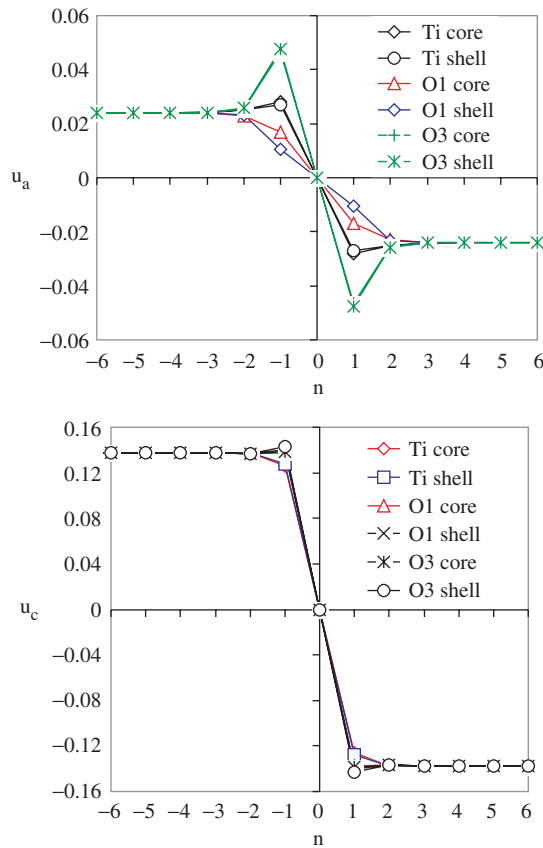


Figure 8. Anharmonic displacements of Ti, O1 and O3 cores and shells for a Ti-centred  $180^\circ$  domain wall.

for  $n \in \mathbb{Z}$ . Here we take advantage of the fact that we can partition the problem into two half space problems with constant coefficient matrices in the governing equations. The final solution will be obtained by matching the two solutions. Let us assume that the Pb, Ti and O1 atoms lying on the domain wall have the index  $n=0$ . For range of interaction  $m$  we have the following bulk governing equations

$$\sum_{\alpha=-m}^m \mathcal{A}_\alpha \mathbf{X}_{n+\alpha} = \mathbf{F}_n \quad n \geq m+1, \quad (51)$$

$$\sum_{\alpha=-m}^m \bar{\mathcal{A}}_\alpha \mathbf{X}_{n+\alpha} = \mathbf{F}_n \quad n \leq -m-1, \quad (52)$$

where  $\mathcal{A}_\alpha$  and  $\bar{\mathcal{A}}_\alpha$  are the stiffness matrices of the right and left sides of the domain wall, respectively. There are  $2m+1$  indices (unit cells) for which governing equilibrium equations should be written separately. For  $m=1$  and  $m=2$  these are indices  $n = -1, 0, 1$  and  $n = -2, -1, 0, 1, 2$ , respectively. For the sake of clarity, we consider

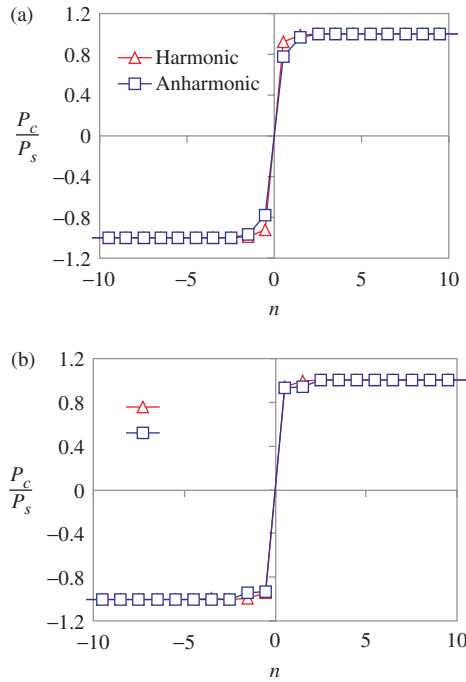


Figure 9. Harmonic and anharmonic polarization distributions for (a) Pb and (b) Ti-centred  $180^\circ$  domain walls.

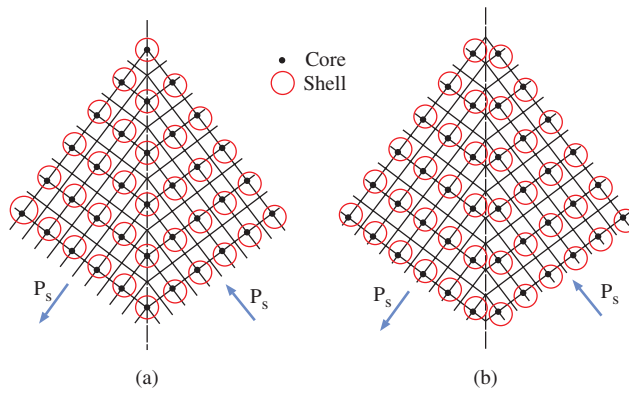


Figure 10. Reference configuration of (a) A cores and shells and (b) O2 cores and shells for an ABO<sub>3</sub>-centred nominal  $90^\circ$  domain wall.

the case  $m = 1$  and then generalizing the results for an arbitrary range of interaction  $m$  would be straightforward.

The bulk governing equations are

$$\mathcal{A}_{-1}\mathbf{X}_{n-1} + \mathcal{A}_0\mathbf{X}_n + \mathcal{A}_1\mathbf{X}_{n+1} = \mathbf{F}_n \quad n \geq 2, \quad (53)$$

$$\bar{\mathcal{A}}_{-1}\mathbf{X}_{n-1} + \bar{\mathcal{A}}_0\mathbf{X}_n + \bar{\mathcal{A}}_1\mathbf{X}_{n+1} = \mathbf{F}_n \quad n \leq -2. \quad (54)$$

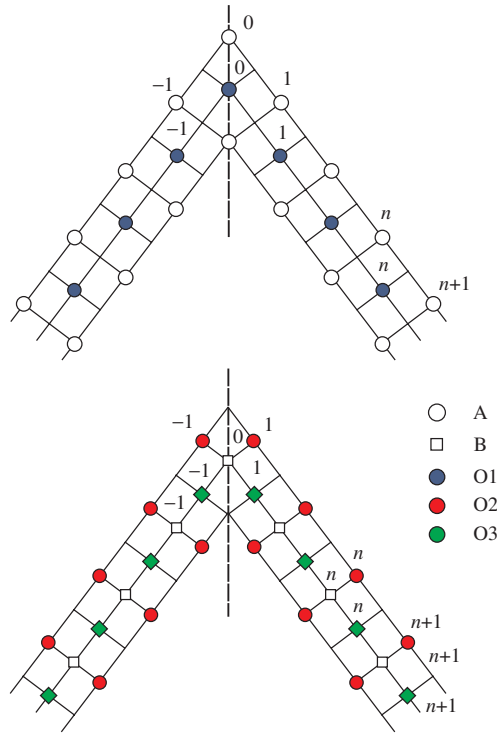


Figure 11. Position and numbering of different atoms in a  $90^\circ$  domain wall in two parallel planes.

The boundary equations are

$$n = -1: \mathcal{A}_{-1}^{(-1)}\mathbf{X}_{-2} + \mathcal{A}_0^{(-1)}\mathbf{X}_{-1} + \mathcal{A}_1^{(-1)}\mathbf{X}_0 = \mathbf{F}_{-1}, \tag{55}$$

$$n = 0: \mathcal{A}_{-1}^{(0)}\mathbf{X}_{-1} + \mathcal{A}_0^{(0)}\mathbf{X}_0 + \mathcal{A}_1^{(0)}\mathbf{X}_1 = \mathbf{F}_0, \tag{56}$$

$$n = 1: \mathcal{A}_{-1}^{(1)}\mathbf{X}_0 + \mathcal{A}_0^{(1)}\mathbf{X}_1 + \mathcal{A}_1^{(1)}\mathbf{X}_2 = \mathbf{F}_1. \tag{57}$$

Note that for  $n=0$  the unit cell consists of only Pb, Ti and O1 atoms. The discrete boundary-value problem can be solved by solving the backward and forward difference equations and matching them on the domain wall.

Unlike the  $180^\circ$  domain wall, the left and right sides of the wall are not symmetrically related. Thus, it would not be possible to fix any atom in the core region; any such constraint would introduce constraint forces and will lead to unphysical solutions. We overcome the translation-invariance issue of the governing equations by relaxing a core region and rigidly translating the two half lattices. In each iteration, unbalanced forces are calculated exactly while displacements of each unit cell are calculated assuming that the adjacent unit cells are fixed. This scheme converged after about two hundred iterations assuming that unbalanced force

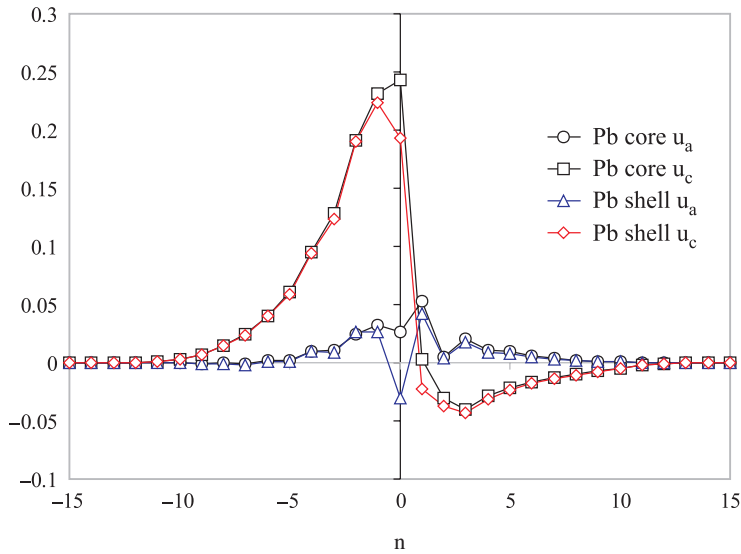


Figure 12.  $a$ - and  $c$ -displacement components for Pb cores and shells in a  $90^\circ$  domain wall.  $n=0$  corresponds to atoms lying on the domain wall in the reference configuration.

tolerance is  $0.05 \text{ eV}/\text{\AA}$ . We find that displacements are nonzero in a core of thickness about 8 nm and the far-field translations are zero.

#### 4.1. Numerical results

Here we present some numerical examples for  $\text{PbTiO}_3$ . Figure 12 shows displacements of Pb cores and shells. It is seen that unit cells  $n > 10$  and  $n < -10$  have negligible displacements and the nonzero displacements are seen mainly for  $-7 \leq n \leq 7$ . This means that the domain wall thickness is about 5 nm. It is also seen that the  $a$ -displacements are about five times smaller than the  $c$ -displacements. Figure 13 shows the  $a$ - and  $c$ -displacements of Ti and O1 cores and shells. The nonzero displacements are supported on a core region of thickness of about 5 nm. Figure 14 shows the  $a$ - and  $c$ -displacements for O2 and O3 cores and shells. Note that the unit cell  $n=0$  does not have O2 and O3 atoms. Again, domain wall thickness is about 5 nm.

### 5. Summary and concluding remarks

We have presented detailed lattice statics calculations for  $180^\circ$  and  $90^\circ$  domain walls in tetragonal  $\text{PbTiO}_3$ . Our treatment of lattice statics is different from other treatments in the literature in that it does not rely on a knowledge of force constants and a fixed number of nearest-neighbour interactions; instead all is needed is an interatomic potential. Our technique can be used for any collection of atoms and is not restricted to lattices. The lattice statics analysis starts from a reference configuration, which is a nominal defect structure. The discrete governing equations are

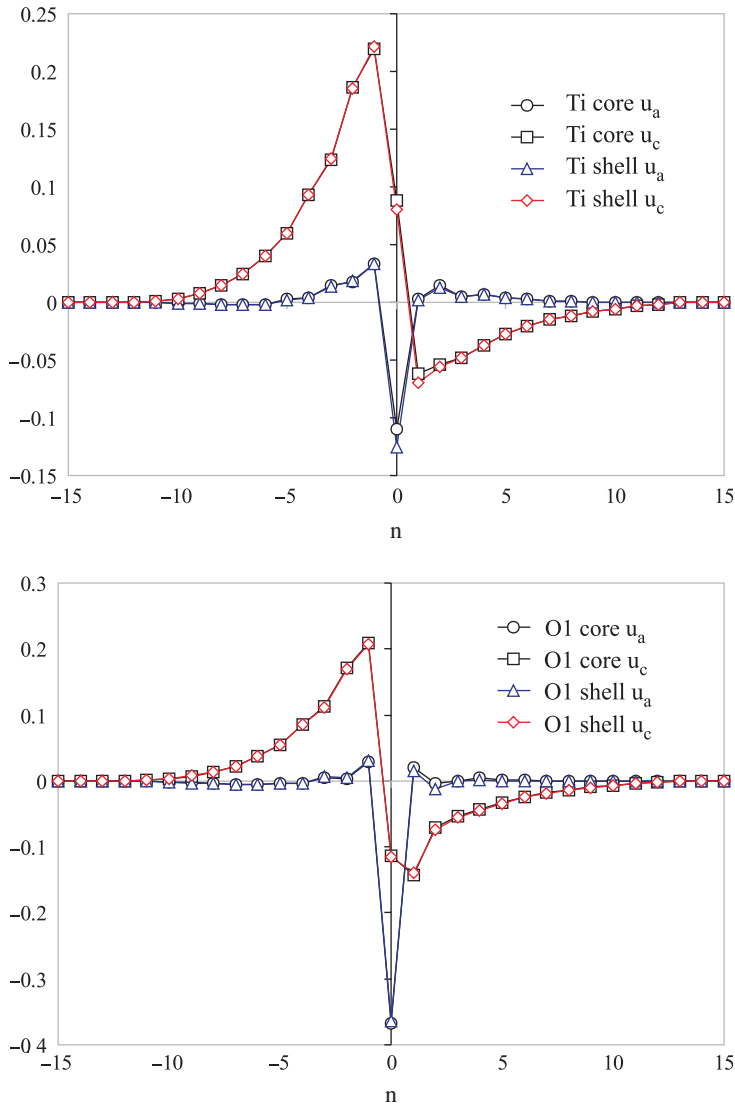


Figure 13.  $a$ - and  $c$ -displacement components for Ti and O1 cores and shells in a  $90^\circ$  domain wall.  $n=0$  corresponds to atoms lying on the domain wall in the reference configuration.

systematically constructed and then are linearized with respect to the reference configuration. The resulting discrete governing equations are linear vector-valued partial difference equations. Using the symmetry of the defective crystal the governing partial difference equations are reduced. In the case of domain walls, the partial difference equations can be reduced to ordinary difference equations. The resulting vector-valued ordinary difference equations with non-constant coefficient matrices are solved using a novel method developed in this paper (see also [30]).

For domain walls the reference configuration is decomposed into equivalence classes, which are infinite sets of atoms of the same type lying on a plane parallel to

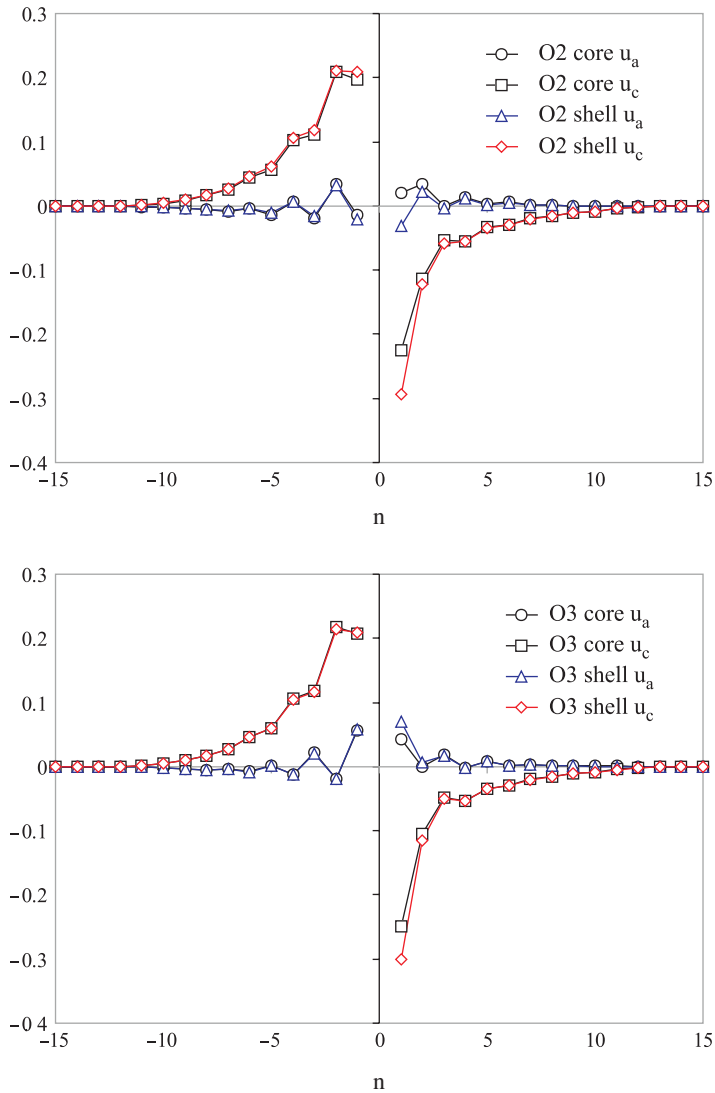


Figure 14.  $a$ - and  $c$ -displacement components for O2 and O3 cores and shells in a  $90^\circ$  domain wall. Note that in our numbering there are no O2 and O3 cores and shells with index  $n=0$  and this is why the graphs are broken at  $n=0$ .

the domain wall. The governing equations are written in terms of interactions of these equivalence classes and this leads to substiffness matrices defined in terms of some lattice sums. We have carefully studied convergence of these lattice sums. Our numerical studies show that shell potentials are extremely localized and this is consistent with previous numerical and experimental studies of ferroelectric domain walls that had suggested atomically sharp domain walls.

We have shown that fully nonlinear solutions can be calculated using a modified Newton–Raphson iteration. The idea is to keep the initial stiffness matrices and

update forces by modifying the reference configuration. In other words, having the first harmonic solution, the reference configuration is modified by superimposing the discrete harmonic displacement field. The new forces are calculated and the scheme is repeated until convergence is accomplished. Convergence of this scheme requires a stable reference configuration. Our reference configurations for both Pb-centred and Ti-centred  $180^\circ$  domain walls are stable as the iterations converged. We studied the structure of  $90^\circ$  domain walls in  $\text{PbTiO}_3$  and fully relaxed a single domain wall in an infinite lattice. We observe that a  $90^\circ$  domain wall is about 5.0 nm thick.

We studied stiffness matrices in the reference configurations of  $180^\circ$  and  $90^\circ$  domain walls and observed that sub-stiffness matrices on the right and left sides of the domain walls are different. This makes the application of discrete Fourier transformation difficult. The harmonic solutions of a homogenized lattice, i.e. those obtained using the average stiffness matrices differ from those of the nonhomogeneous lattice by about forty percent. However, the final nonlinear solutions are exactly the same. This shows that using the homogenized lattice is a good approximation. We observe very sharp domain walls in the order of 1 nm and 5 nm for  $180^\circ$  and  $90^\circ$  domain walls, respectively. This is in qualitative agreement with the *ab initio* calculations of domain walls in  $\text{PbTiO}_3$  and also with the recent experimental observations. We emphasize that in our method we do not assume any artificial periodicity and analyse single  $180^\circ$  and  $90^\circ$  domain walls.

The methods and accomplishments of this paper can be summarized as follows.

- The discrete governing equations of a defective multilattice are systematically constructed with no restrictions on the range of interactions.
- The (nonlinear) discrete governing equations are linearized about an arbitrary reference configuration and not necessarily about the bulk crystal.
- The order of the governing vector-valued partial difference equations are systematically reduced exploiting the symmetry of the defective multilattice. In the case of domain walls, the discrete governing equations are reduced to vector-valued ordinary difference equations.
- This paper formulates the problem of domain walls as a discrete boundary-value problem. The discrete boundary-value problem of a single  $180^\circ$  domain wall in an infinite crystal is solved analytically.
- The fully nonlinear solutions are obtained by using modified Newton–Raphson iterations.
- Several numerical examples are given for  $\text{PbTiO}_3$ . We observe that  $180^\circ$  and  $90^\circ$  domain walls are about 1 nm and 5 nm thick, respectively.

The method developed here has several potential applications. For example, this method can be used in understanding the interaction of different types of defects, e.g. effect of oxygen vacancies on domain wall structure. This method can also be used in studying more complicated defects like steps in  $180^\circ$  domain walls. An interesting extension of this method is to consider the effect of finite temperatures on defect structure, i.e. a generalization of lattice dynamics for defective crystals. This would be particularly important as molecular dynamics simulations, even if available for a defective system, are not reliable for low temperatures. These would be the subject of future work and will be discussed in future communications.



## Acknowledgements

We benefited from numerous discussions with R. Cohen, A. Asthagiri, S. Akber, W. A. Goddard, T. Cagin and Q. Zhang. The financial support of the Army Research Office under MURI grant No. DAAD19-01-1-0517 is gratefully acknowledged.

### A. Long-range forces

As ferroelectric perovskites are ionic crystals, Coulombic interactions play a key role in determining their structure and equilibrium configurations. Unlike all the existing methods, in this paper we do not assume any periodicity and consider a single defect in an infinite crystal. Therefore, the calculation of the energy, forces and stiffnesses should be studied carefully. In this appendix, we briefly discuss the standard methods of calculating the energy and force for Coulombic interactions and some recent developments for nonperiodic systems and numerically show that care must be taken in the case of nonperiodic systems.

Long-range forces are forces that come from Coulombic interactions. The usual practice is to first assume a periodic system and find an expression for the energy of a unit cell using Ewald summation technique and then find the force vectors by taking the appropriate partial derivatives. However, the problems we study in this paper are not periodic, and we have to explore other methods. We use a method proposed by Wolf and his coworkers [25], and examine it against the Ewald summation in the following.

In a recent paper, Wolf *et al.* [25] studied the Madelung problem, i.e. the divergence associated with the  $r^{-1}$  term in the Coulomb potential of condensed ionic systems, by direct summation. Earlier Wolf [34, 35] had observed that the effective Coulombic potential of ions in condensed systems is short-ranged and falls off as  $r^{-5}$ . Based on this and similar observations by others, Wolf *et al.* [25] developed a numerical method for calculating the Madelung energy by direct summation in direct space. Their idea is to consider spherical shells of increasing radii and calculate the electrostatic energy of corresponding neutralized spherical balls. It is assumed that the total charge of a given spherical ball is concentrated on its boundary sphere instead of in a layer of thickness equal to the length of the shift vector (for a multilattice of two simple lattices like NaCl). For NaCl lattice, they numerically show that the sequence of energies of the neutralized spherical balls approaches to the Madelung energy of the infinite lattice in an oscillatory way. They show that neutralizing a spherical ball is equivalent to radially projecting every charge inside the ball on the boundary sphere with the opposite charge. It is important to note that their projection is not unique; while putting the neutralizing charges anywhere on the sphere gives the same Madelung energy, the forces (and higher derivatives of the energy) depend on the position of neutralizing charges. Further, it is not clear to us why Wolf's projection should give the correct forces. However, in all the existing numerical examples it gives the correct answer.

### A1. Wolf's method

Let us briefly review the method introduced by Wolf *et al.* [25] for a classical Coulombic potential. Consider a charge  $i$  with position vector  $\mathbf{x}_i$  (this could be a core or a shell charge) and a spherical shell with radius  $R_c$  centred at  $\mathbf{x}_i$ . We consider only those charges that lie inside the sphere. In general, the collection of charges inside the sphere is not charge neutral. The energy of ion  $i$  for the cut-off radius  $R_c$  is

$$\mathcal{E}_i(R_c) = \frac{1}{2} \sum_{\substack{j \neq i \\ |\mathbf{x}_{ij}| < R_c}} \frac{Q_i Q_j}{|\mathbf{x}_{ij}|}, \quad (58)$$

where  $\mathbf{x}_{ij} = \mathbf{x}_i - \mathbf{x}_j$  is the relative position vector. It should be noted that this energy does not converge to the correct Madelung energy as  $R_c \rightarrow \infty$  because of the lack of charge neutrality. Wolf *et al.* [25] resolve this problem by considering a sequence of charge-neutralized spheres. It is assumed that the net charge is concentrated on the boundary of the sphere. The neutralized potential can be written as

$$\mathcal{E}_i^{\text{neut.}}(R_c) = \frac{1}{2} \sum_{\substack{j \\ |\mathbf{x}_{ij}| < R_c}} \frac{Q_i Q_j}{R_c}. \quad (59)$$

Note that this includes the term  $i=j$ . Also note that the net charge is

$$\Delta Q_i(R_c) = \sum_{\substack{j \\ |\mathbf{x}_{ij}| < R_c}} Q_j. \quad (60)$$

Neutralizing a given sphere is equivalent to radially projecting each charge on the sphere with the opposite sign.

**Remark:** Given two point charges  $q_i$  and  $q_j$  located at points  $\mathbf{x}_i$  and  $\mathbf{x}_j$ , respectively, Wolf *et al.* [25] define a shifted Coulomb potential by

$$V_{sh}(r_{ij}) = \begin{cases} q_i q_j / r_{ij} - q_i q_j / R_c & r_{ij} < R_c, \\ 0 & r_{ij} > R_c. \end{cases} \quad (61)$$

They then rewrite the shifted potential as

$$V_{sh}(r_{ij}) = \begin{cases} q_i q_j / r_{ij} - \lim_{r_{ij} \rightarrow R_c} q_i q_j / r_{ij} & r_{ij} < R_c, \\ 0 & r_{ij} > R_c, \end{cases} \quad (62)$$

which is a bit misleading as this should be written as

$$V_{sh}(r_{ij}) = \begin{cases} q_i q_j / r_{ij} - \lim_{\xi \rightarrow R_c} q_i q_j / \xi & r_{ij} < R_c, \\ 0 & r_{ij} > R_c. \end{cases} \quad (63)$$

In their equation (3.17) they argue that

$$\frac{dV_{sh}(r_{ij})}{dr_{ij}} = -\frac{q_i q_j}{r_{ij}^2} + \frac{q_i q_j}{R_c^2} \quad r_{ij} < R_c. \quad (64)$$

This means that they implicitly assume in (62) that

$$\frac{d}{dr_{ij}} \left( \lim_{r_{ij} \rightarrow R_c} \frac{q_i q_j}{r_{ij}} \right) = \lim_{r_{ij} \rightarrow R_c} \frac{d}{dr_{ij}} \left( \frac{q_i q_j}{r_{ij}} \right), \quad (65)$$

which is mathematically meaningless. Note that accepting (64) implies that for  $r_{ij} < R_c$

$$V_{sh}(r_{ij}) = \frac{q_i q_j}{r_{ij}} + \frac{q_i(q_j r_{ij}/R_c)}{R_c}, \quad (66)$$

i.e. for calculating force the projected charge for  $q_j$  is  $q_j r_{ij}/R_c$ . This means that in Wolf's method energy and force are calculated using two different auxiliary systems, one with neutralizing charges  $-q_j$  for energy and one for auxiliary charges  $q_j r_{ij}/R_c$  for force. One should also note that the energy is invariant with respect to any rearrangement of neutralizing charges on the sphere of radius  $R_c$ .

Now considering the two separate auxiliary neutralized systems of charges, the electrostatic energy of the charge  $i$  is

$$\mathcal{E}_i^{\text{tot.}}(R_c) = \frac{1}{2} \sum_{\substack{j \neq i \\ |\mathbf{x}_{ij}| < R_c}} \frac{Q_i Q_j}{|\mathbf{x}_{ij}|} - \frac{1}{2} \sum_{|\mathbf{x}_{ij}| < R_c} \frac{Q_i Q_j}{R_c}. \quad (67)$$

The force (calculated by Wolf's method) on charge  $i$  can be written as

$$\mathbf{f}^i = -\frac{1}{2} \sum_{\substack{j \neq i \\ |\mathbf{x}_{ij}| < R_c}} \frac{\partial}{\partial \mathbf{x}^i} \frac{Q_i Q_j}{|\mathbf{x}_{ij}|} + \frac{1}{2} \sum_{\substack{j \neq i \\ |\mathbf{x}_{ij}| < R_c}} \left( \frac{\partial}{\partial \mathbf{x}^i} \frac{Q_i Q_j}{|\mathbf{x}_{ij}|} \right)_{|\mathbf{x}_{ij}|=R_c}. \quad (68)$$

### A2. Damped Wolf's method

We explain the damped Wolf's method for the classical Coulombic potential and numerically investigate its validity in terms of convergence of the energy and force for tetragonal  $PbTiO_3$  using the SC classical shell potential. In the damped method the complementary error function is used as the damping function. The only reason for choosing this function, besides the required properties it has, is that this is the same damping function used in the classical Ewald summation method. The energy of the  $i$ th charge can be written as

$$\mathcal{E}^i = \frac{1}{2} \sum_{j \neq i} \frac{Q_i Q_j \operatorname{erfc}(\alpha |\mathbf{x}_{ij}|)}{|\mathbf{x}_{ij}|} + \frac{1}{2} \sum_{j \neq i} \frac{Q_i Q_j \operatorname{erf}(\alpha |\mathbf{x}_{ij}|)}{|\mathbf{x}_{ij}|}, \quad (69)$$

where  $\alpha$  is a damping parameter and  $\operatorname{erfc}(x) = 1 - \operatorname{erf}(x)$  is the complementary error function. Now the idea is to decompose the energy into two parts such that one part

is negligible. The above decomposition does not have this property because the second term becomes very large for large values of  $\alpha$ . However adding the term corresponding to  $i=j$  and subtracting it from the first term would make (69) what we need. Thus

$$\mathcal{E}_{\text{sphere}}^i(R_c) \approx \frac{1}{2} \sum_{\substack{j \neq i \\ |\mathbf{x}_{ij}| < R_c}} \frac{Q_i Q_j \operatorname{erfc}(\alpha |\mathbf{x}_{ij}|)}{|\mathbf{x}_{ij}|} - \frac{\alpha}{\sqrt{\pi}} Q_i^2. \quad (70)$$

The energy of the neutralizing charges is

$$\mathcal{E}_{\text{neut}}^i(R_c) = \frac{1}{2} \frac{Q_i \Delta Q_i(R_c) \operatorname{erfc}(\alpha R_c)}{R_c}. \quad (71)$$

Therefore, the energy for a cut-off radius  $R_c$  is

$$\begin{aligned} \mathcal{E}^i(R_c) = \frac{1}{2} \sum_{\substack{l \neq i \\ |\mathbf{x}_{ij}| < R_c}} & \left[ \frac{Q_i Q_j \operatorname{erfc}(\alpha |\mathbf{x}_{ij}|)}{|\mathbf{x}_{ij}|} - \frac{Q_i Q_j \operatorname{erfc}(\alpha R_c)}{R_c} \right] \\ & - \left( \frac{\operatorname{erfc}(\alpha R_c)}{2R_c} + \frac{\alpha}{\sqrt{\pi}} \right) Q_i^2. \end{aligned} \quad (72)$$

### A3. Comparison between the Wolf and Ewald methods

We have performed the following numerical tests for tetragonal  $\text{PbTiO}_3$ . The calculated unit-cell energy using Wold's method, Ewald and the damped Wolf's method for different values of the damping parameter are compared in figure 15. It is interesting that in the damped Wolf's method the energy is very sensitive to the damping parameter and there is a very small interval of  $\alpha$  that gives the correct energy.

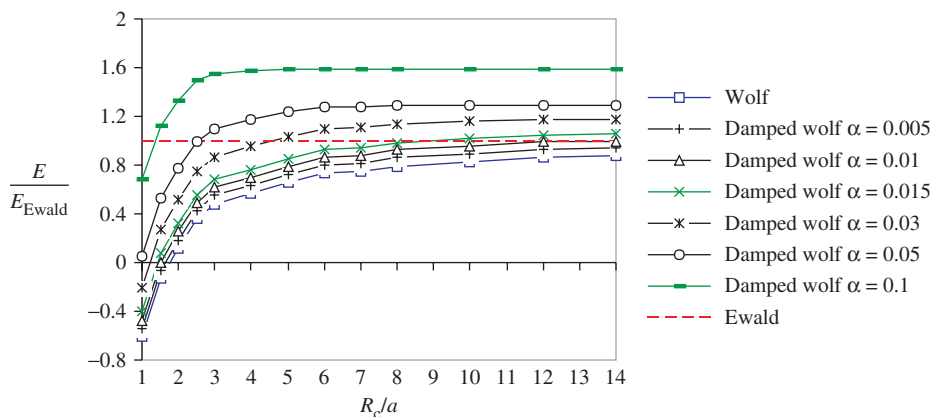


Figure 15. Unit cell electrostatic energy in  $\text{PbTiO}_3$  using Ewald, Wolf and damped Wolf methods.

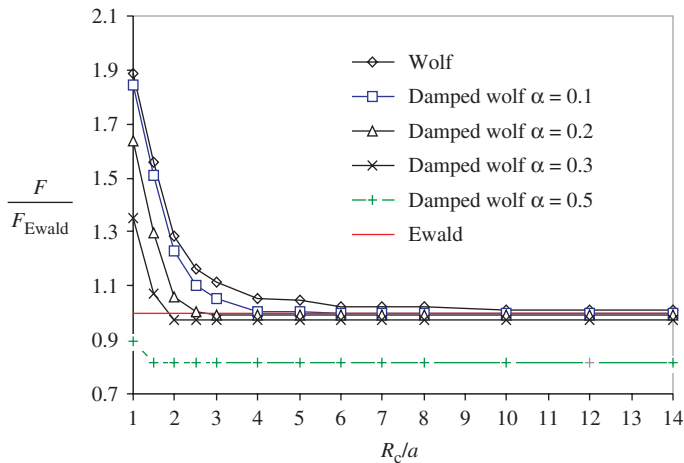


Figure 16. Pb core force in tetragonal direction in  $\text{PbTiO}_3$ .

The optimum values are  $\alpha \simeq 0.01$ . Wolf's method does not have a good convergence as the calculated energy does not converge to its correct values even for  $R_c = 14a$ . The other thing to note is that convergence is not oscillatory unlike that of the NaCl lattice studied by Wolf and his co-workers.

Pb core forces calculated using Wolf, Ewald and damped Wolf are compared in figure 16. Here a larger interval of  $\alpha$  is acceptable and the optimum value is  $\alpha \simeq 0.2$ . Wolf's method is very slowly convergent and hence not practically useful.

## References

- [1] J. Valasek, *Phys. Rev.* **17** 475 (1921).
- [2] R.E. Cohen and H. Krakauer, *Ferroelectrics* **136** 65 (1992).
- [3] D. Damjanovic, *Rep. Prog. Phys.* **61** 1267 (1998).
- [4] M. Kamlah, *Continuum Mech. Thermodynam.* **13** 219 (2001).
- [5] K. Bhattacharya and G. Ravichandran, *Acta Mater.* **51** 5941 (2003).
- [6] F. Jona and G. Shirane, *Ferroelectric Crystals* (Dover, New York, 1993).
- [7] W. Kanzig, *Sol. Stat. Phys. – Advan. in Research and Appl.* **4** 1 (1957).
- [8] S. Stemmer, S.K. Streiffer, F. Ernst, *et al.*, *Phil. Mag. A* **71** 713 (1995).
- [9] N. Floquet, C.M. Valot, M.T. Mesnier, *et al.*, *J. Physique III* **7** 1105 (1997).
- [10] M. Foeth, A. Sfera, P. Stadelmann, *et al.*, *J. Electron Microsc.* **48** 717 (1999).
- [11] D. Shilo, G. Ravichandran and K. Bhattacharya, *Nat. Mater.* **3** 453 (2004).
- [12] W.W. Cao and L.E. Cross, *Phys. Rev. B* **44** 5 (1991).
- [13] V.A. Zhirnov, *Sov. Phys. JETP – USSR* **8** 822 (1959).
- [14] X.R. Huang, X.B. Hu, S.S. Jiang, *et al.*, *Phys. Rev. B* **55** 5534 (1997).
- [15] W.N. Lawless, *Phys. Rev.* **175** 619 (1968).
- [16] B. Meyer and D. Vanderbilt, *Phys. Rev. B* 6320 (2001).
- [17] J. Padilla, W. Zhong and D. Vanderbilt, *Phys. Rev. B* **53** R5969 (1996).
- [18] S. Poykko and D.J. Chadi, *Appl. Phys. Lett.* **75** 2830 (1999).
- [19] S. Poykko and D.J. Chadi, *J. Phys. Chem. Sol.* **61** 291 (2000).
- [20] T.J. Matsubara, *J. Phys. Soc. Jpn* **7** 270 (1952).
- [21] H. Kanazaki, *J. Phys. Chem. Sol.* **2** 24 (1957).
- [22] M. Born and K. Huang, *Dynamical Theory of Crystal Lattices* (Oxford, New York, 1988).

- [23] V.K. Tewary, Adv. Phys. **22** 757 (1973).
- [24] M. Ortiz and R. Phillips, Adv. Appl. Mechan. **59** 1217 (1999).
- [25] D. Wolf, P. Keblinski, S. R. Phillpot, *et al.*, J. Chem. Phys. **110** 8254 (1999).
- [26] B.G. Dick and A. W. Overhauser, Phys. Rev. **112** 90 (1958).
- [27] M. Sepliarsky, Z. Wu, A. Asthagiri, *et al.*, Ferroelec. **301** 55 (2004).
- [28] A. Asthagiri, Z. Wu, N. Choudhury, *et al.*, Ferroelec. **333** 69 (2006).
- [29] M. Sepliarsky and R.E. Cohen, in *Fundamental Physics of Ferroelectrics* (American Institute of Physics, NY), edited by R.E. Cohen (2002), pp. 36–44.
- [30] A. Yavari, M. Ortiz and K. Bhattacharya, J. Elasticity **86** 41 (2007).
- [31] P.P. Ewald, Ann. Phys. **64** 253 (1921).
- [32] A. Yavari, Atomic structure of ferroelectric domain walls, free surfaces and steps. PhD thesis, California Institute of Technology (2004).
- [33] R. Resta, Model. Simul. Mater. Sci. Engng. **11** R69 (2003).
- [34] D. Wolf, Phys. Rev. Lett. **68** 3315 (1992).
- [35] D. Wolf, Springer Proc. Phys. **80** 57 (1995).